

From larger-scale cold-gas angular-momentum environment to galaxy star-formation activeness

SEN WANG,¹ DANDAN XU,¹ AND SHENGDONG LU²

¹*Department of Astronomy, Tsinghua University, Beijing, 100084, China*

²*Institute for Computational Cosmology, Department of Physics, University of Durham, South Road, Durham, DH1 3LE, UK*

ABSTRACT

We study the influence of the ambient large-scale cold-gas vorticity on the specific star formation rate (sSFR) of all central galaxies with stellar masses of $10.0 < \log M_*/M_\odot < 11.5$, using the IllustrisTNG-100 simulation. The cold-gas vorticity defined and calculated for gas with $T_{\text{gas}} < 2 \times 10^4 \text{K}$ and on scales of $\sim 1 \text{Mpc}$ can well describe the angular motion of the ambient cold gas. We find crucial evidence for a clear connection between the cold gas spin/vorticity and star formation activeness, in that at any given halo mass, galaxies that live in a higher cold-gas vorticity environment are generally less actively star forming, regardless of the large-scale environment type (filament or knot) the galaxy lives in, or it being star-forming or quenched. In particular, at any fixed halo mass scale, the environmental cold-gas vorticities of galaxies in filaments are generally higher than those of galaxies in knots, naturally explaining lower the sSFRs of filament galaxies than of knot galaxies. This large-scale cold-gas vorticity is also highly connected to the orbital angular momentum of environmental galaxies up to a distance of $\sim 500 \text{kpc}$, indicating their common origin and/or possible angular momentum inheritance/modulation from the latter to the former. The negative modulation by the environmental vorticity to galaxy star formation is only significantly observed for the cold gas, indicating the unique role of cold-gas angular momentum.

Keywords: methods: numerical, methods: statistical, galaxies: evolution, galaxies: formation

1. INTRODUCTION

The angular momentum environment of galaxies plays an important role in shaping and regulating a variety of galaxy properties, including their morphologies, kinematics, as well as star formation activities (e.g., Fall & Efstathiou 1980; Mo et al. 1998; Teklu et al. 2015; Zavala et al. 2016; Rodriguez-Gomez et al. 2017; Zeng et al. 2021; Lu et al. 2021; Wang et al. 2022; Lu et al. 2022b,a; Valenzuela & Remus 2024; Hu et al. 2024; Gámez-Marín et al. 2024). Such angular momentum environments can refer to a wide range of angular momentum properties, for example, the theoretical halo and galaxy spins (e.g., Peebles 1969; Mo et al. 1998; Bullock et al. 2001; Bett et al. 2007), the observed stellar angular momentum (e.g., Emsellem et al. 2011; Romanowsky & Fall 2012; Cortese et al. 2016), the in-spiral motion of the circum-

galactic gas (e.g., Stewart et al. 2011; Ho et al. 2017; Zhang et al. 2023), the orbital angular momentum of neighbouring galaxies at distances up to sub-Mpc scales (Libeskind et al. 2012, 2014b; Danovich et al. 2015; Lu et al. 2022b; Wang et al. 2022, 2024; Valenzuela & Remus 2024), as well as the cosmic vortical flow and filamentary accretion on Mpc scales (e.g., Pichon & Bernardeau 1999; Pichon et al. 2011; Libeskind et al. 2013a,b; Danovich et al. 2012; Stewart et al. 2013; Hahn et al. 2015; Laigle et al. 2015; Lu et al. 2024). We have come a long way understanding the many processes and mechanisms related to the formation and evolution of these angular momentum properties.

In the current paradigm, the initial angular momentum of a dark matter halo is not a result of primordial velocity *vector* perturbation, which would soon decay due to the cosmic expansion (Jones 1976; Gott 1977; Efstathiou & Silk 1983; Bernardeau et al. 2002), but a consequence of a torque moment exerted by a shear, curl-free, potential flow of the ambient large-scale structure in the linear or quasi-linear regime prior to the gravitational collapse of the region, as is explained by the tidal torque theory (e.g., Peebles 1969; Doroshkevich 1970; Fall & Efstathiou 1980; White 1984;

Corresponding author: Sen Wang
wangsen19@mails.tsinghua.edu.cn

Corresponding author: Dandan Xu
dandanxu@tsinghua.edu.cn

Barnes & Efstathiou 1987; Catelan & Theuns 1996; Schäfer 2009, and also see Liao et al. 2017; Neyrinck et al. 2020). In an isolated scenario, this angular momentum is conserved during the collapse after turnaround. Gas condenses within the dark matter halo, forming gaseous discs where star formation happens. The newly formed stellar disc is therefore expected to retain a large fraction of the specific angular momentum of the dark matter halo (e.g., White & Rees 1978; Mo et al. 1998; Firmani & Avila-Reese 2000, 2009; Romeo et al. 2023).

In reality, however, galaxies live and flow in the cosmic web. Their angular momentum acquisition, in particular that is associated with the cold stream accretion in filamentary structures, can also be influenced by the rich dynamics due to a high level of non-linearity of the cosmic web on large scales. This effect can be particularly strong at high redshifts (Pichon et al. 2011; Danovich et al. 2012; Codis et al. 2012; Libeskind et al. 2013b; Danovich et al. 2015; Laigle et al. 2015; Tillson et al. 2015; Lu et al. 2024). In addition, galaxies in their dark matter halos also strongly interact and merge among themselves to grow more massive structures in a hierarchical fashion. These highly non-linear processes of galaxy mergers and flybys also largely influence the growth of angular momentum (e.g., Vitvitska et al. 2002; Maller et al. 2002; Hetzner & Burkert 2006; Bois et al. 2011; Welker et al. 2014; Bett & Frenk 2016). These processes can not only change the angular momenta of dark matter halo and stellar discs, but also inject angular momentum into the circumgalactic medium (CGM), in particular the cold CGM gases that are accreted to galaxies (e.g., Stewart et al. 2011, 2013; Wang et al. 2022; Lu et al. 2022b). We shall also note that apart from the variety of dynamical effects due to gravitation as discussed above, kinetic and thermal feedback of baryons can also change a galaxy’s angular momentum environment (e.g., Maller & Dekel 2002; Bett et al. 2010; Sharma et al. 2012; Genel et al. 2015; DeFelippis et al. 2017) by altering the angular momentum distribution of any given species or transferring angular momenta among different species (see e.g., Zavala et al. 2016; Zjupa & Springel 2017).

In this study, we focus on a specific type of angular momentum modulation that is closely related to the galaxy interaction environment and the large-scale vortical flow. In particular, we study the impact of this angular momentum environment on galaxy star formation activities. In a recent paper series (Wang et al. 2022; Lu et al. 2022b), we already carried out a pilot study using typical star-forming and quenched galaxy samples from the TNG-100 simulation (Marinacci et al. 2018; Naiman et al. 2018; Springel et al. 2018; Nelson et al. 2018, 2019a; Pillepich et al. 2018, 2019). We found that the CGM and the ambient galaxy environment around present-day quenched galaxies tend to have higher spins and higher orbital angular momenta than those of star-forming

galaxies (within a similar mass range). Our interpretation of that finding was that a higher CGM gas spin, as inherited from interacting galaxies in the neighbourhood, can prevent efficient gas infall to fuel central star formation. In term of the massive red and dead galaxies, this provides a mechanism that keeps a galaxy quenched (once it is quenched), which is complementary to the AGN feedback quenching mechanism (e.g., Granato et al. 2004; Hopkins et al. 2005; Di Matteo et al. 2005, 2008; Croton et al. 2006; Cattaneo et al. 2009).

In this study, we aim at looking for stronger evidence using the simulation for a close connection between a galaxy’s star formation activeness and its ambient angular momentum environment. Regarding our previous studies, there are three aspects worth noting. Firstly, both quenching and halo spin correlate positively with galaxy/halo mass, and the observed connection between spin and star formation rate (SFR) could merely be a consequence of such mass dependencies, although though in Lu et al. (2022b) we adopted a few different definitions of spin in order to eliminate so. Secondly, only the cold gas (e.g., with an effective temperature T_{gas} below $\sim 2 \times 10^4$ K as defined in our previous studies) is truly relevant for star formation. Therefore the spin in question is not the halo spin, not the total gas spin, but some spin property of the cold gas. Thirdly, from a gas acquisition perspective, the cold circumgalactic gas at larger scales is often highly localized in the form of extended streams, sometimes accreted from the intergalactic medium associated with filamentary structures, and sometimes stripped from incoming satellite galaxies (e.g., see Figure 7 and 8 in Wang et al. 2022 and the related discussion therein). Therefore conventionally defined spin parameters (e.g., Bullock et al. 2001) are not suited to capture such angular momentum behaviors.

Due to these reasons, we need to find a better definition for “spin” that can describe the angular motion of the ambient cold gas at larger distances, which shall also not necessarily be confined to a halo’s domain. We therefore adopt the velocity vorticity $\nabla \times v$ for the cold gas on a spatial scale of ~ 1 Mpc. We note that the vorticity field of the cosmic matter flow is a result of higher-order perturbation developed in the highly non-linear regime. It has been well studied and found to be largely responsible for halo angular momentum growth during the non-linear evolution phase at high redshifts (e.g., Pichon & Bernardeau 1999; Bernardeau et al. 2002; Wang et al. 2014), and also to explain the alignment between halo spins and the large scale structures (e.g., Libeskind et al. 2013b; Hahn et al. 2015; Laigle et al. 2015). In this study, we also investigate this quantity but for the ambient cold gas at larger scales, and take this as a more general depiction of its angular motion. While the choice of 1 Mpc is motivated by our previous studies (Wang et al. 2022; Lu et al. 2022b) which have demonstrated that the cold circumgalactic gas (with an in-spiraling streaming motion at distances

of ~ 300 kpc scales), as influenced by the angular momentum environment on larger scales, can substantially regulate the efficiency of the cold gas infall from that large distances. In many occasions, such an angular momentum modulation, is closely related to galaxy/subhalo interaction and merger that happen at that large distances, which help to enhance the CGM angular momentum in question.

With this, we can now, at a more fundamental level, search for clear evidence for connections between the cold gas spin/vorticity and star formation activeness. Specifically, we switch the perspective from specific angular momentum of CGM up to ~ 300 kpc and gravitationally bounded to galaxy halos as in our previous studies (Wang et al. 2022; Lu et al. 2022b), to the cold-gas vorticity of the cosmic environment on ~ 1 Mpc scale as in this study. We find that at any given mass, galaxies that live in a higher cold-gas vorticity environment are generally less actively star forming. We also study how this cold gas vorticity may vary in different large-scale cosmic environments and find that at any fixed halo mass scale, the environmental cold-gas vorticity in filaments are generally higher than that in knots, naturally explaining lower sSFRs in filament galaxies than in knot galaxies. We also demonstrate that this quantity, as expected, is highly connected to the orbital motions of galaxies in the vicinity (also see Libeskind et al. 2014b), indicating their common origins and a possible angular momentum inheritance/modulation from the latter to the former. We show that such a negative modulation by the angular momentum environment to galaxy star formation is only significantly observed for the cold gas, but not for either the total matter or the total gas component, indicating the unique role of cold gas. We emphasize that the angular/vortical motion of the cold gas on large scales, is a crucial element shaping the star-forming and quenching status of a galaxy; the cold-gas vorticity field is thus an important feature, among others, to depict a galaxy's larger-scale environment, in particular when studying its impact on galaxy evolution.

This paper is organized as follows: In Section 2, we present the simulation details and illustrate the on-mesh definitions of a number of properties and the method that we use to classify large-scale structures. In Section 3, we re-visit our typical galaxy samples from previous works and emphasize the uniqueness of cold gas. We then study the cold gas vorticity environment of general galaxy samples and samples with different star formation states and environment types in Section 4. Finally discussion and conclusions are given in Section 5 and 6, respectively. Throughout the paper, we adopt the same cosmology as those used in the IllustrisTNG simulation (i.e., based on the Planck results Planck Collaboration et al. 2016), with a total matter density of $\Omega_m = 0.3089$, a baryonic matter density of $\Omega_b = 0.0486$, and a Hubble con-

stant $h = H_0/(100 \text{ km s}^{-1} \text{ Mpc}^{-1}) = 0.6774$, assuming a flat Λ CDM universe.

2. METHODOLOGY

2.1. The simulation

The Next Generation Illustris Simulations (IllustrisTNG, TNG hereafter; Marinacci et al. 2018; Naiman et al. 2018; Springel et al. 2018; Nelson et al. 2018, 2019a; Pillepich et al. 2018, 2019) are a suite of magneto-hydrodynamic cosmological simulations implemented by the moving-mesh code AREPO (Springel 2010) for galaxy formation and evolution. In this paper, following the previous works, we use IllustrisTNG-100 (TNG-100 hereafter), which carries a periodic box of side length of 110.7 Mpc with mass resolutions of $7.5 \times 10^6 M_\odot$ and $1.4 \times 10^6 M_\odot$ for the dark matter (DM) and the baryon. The gravitational softening length is $0.5 h^{-1} \text{ kpc}$ for the dark matter and stellar particles. The host halos are identified using SUBFIND algorithm (Springel et al. 2001; Dolag et al. 2009). The outputs of galaxies and halos of all 100 snapshots are available through the public data access (Nelson et al. 2019b) of TNG project¹.

2.2. Specific SFR, over-density, vorticity on the grid

The goal of this study is to identify and understand the correlation between the large-scale angular momentum field in the form of the flow vorticity on a scale of ~ 1 Mpc (see Section 1 for the motivation of choosing this scale) and the galaxy star formation activeness. For this reason, we have implemented a grid mesh of 128^3 to cover the entire simulation box of $(110.7 \text{ Mpc})^3$ with spatial resolution of ~ 865 physical kpc. This is our basic mesh setup, which is used to calculate several fields, including (1) specific star formation rate (sSFR, as contributed by all central galaxies), (2) total matter over-density, (3) velocity vorticity, and (4) large-scale environmental type. We note that the grid cells themselves are also used as statistical samples.

We have first computed the sSFR on the grid. To do so, we choose all central galaxies at redshift $z = 0$ (snapshot 099) and add their stellar masses and SFRs to the grid using the near-grid point (NGP) assignment. The ratio of the two gives the sSFR of the grid point. We have then calculated the matter over-density field, defined as $\delta \equiv \rho_m/\bar{\rho}_m - 1 = \rho_m/(\Omega_m \rho_{cr}) - 1$, where ρ_{cr} is the critical density of the universe. For this calculation, we take all particles at redshift $z = 0$ and assign them to the grid according to the *Clouds in Cells* (CIC) algorithm.

In addition, we have introduced the vorticity field ω . In previous works (Wang et al. 2022; Lu et al. 2022b), the authors identified the environmental modulation to the CGM

¹ <http://www.tng-project.org/data/>

angular momentum (i.e. positive correlation between satellites orbital angular momentum and CGM angular momentum, see Figure 4 in Lu et al. 2022b) and a further influence of such angular momentum to the sSFR of galaxies (i.e. the lower angular momentum in the CGM, the higher sSFR, see Figure 5 in Wang et al. 2022 and Figure 2, 3 in Lu et al. 2022b). Here, we would like to generalize such a “angular momentum” property and relate it to the concept of cosmic vortical flow on large scales (Pichon & Bernardeau 1999; Wang et al. 2014; Libeskind et al. 2013b; Hahn et al. 2015).

According to the Helmholtz Decomposition Theorem, one can extract the rotational parts of a general vector field by applying a curl operator to the field. Considering the kinetic motion of a region, this “rotation” can be directly defined as the curl of the velocity field \mathbf{v} , namely the vorticity field $\boldsymbol{\omega} \equiv \nabla \times \mathbf{v}$. In this study, we particularly compute the vorticity field $\boldsymbol{\omega}$ for three types of components, i.e., total matter, total gas, and the cold gas. Specifically, we follow Wang et al. (2022) and define the cold gas as gases with effective temperature $T_{\text{gas}} < 2 \times 10^4 \text{K}$, where the cooling function peaks. Each time we take all particles, or total gas cells, or the cold-gas cells alone, and assign them to the grid. The vorticity field $\boldsymbol{\omega}$ calculated on the mesh essentially reveals the surrounding (grid scale) “rotational” motion relative to the target grid point.

In this study, we focus on the influence of the angular momentum environment particularly from the diffuse cold gases on larger scales, instead of those in the close vicinity to any galaxies. This is because the central gas motion as well as its relation with star formation activeness can be largely affected by feedback processes, which are implemented differently among different simulations. To avoid of such contamination, we therefore have also excluded all the cold gas elements that are gravitationally bound within 1/3 of any galaxy’s r_{200} (the radius within which the mean mass density is 200 times the critical density of the universe). We have verified that all results calculated in this case remain the same qualitatively as using all cold gas elements. For this reason, in all figures below, we present results using all cold gas elements in the simulation, except for Fig. 6 where comparisons between the two cases are presented as a demonstration.

2.3. Cosmic web construction and classification

In order to understand the cold-gas vorticity modulation in different large-scale structure environment, we have also classified the cosmic web structure of the simulation into four basic types, i.e., knot, filament, sheet, and void. There have been many methods developed for such classification schemes, for example, using the Hessian of the gravitational potential (Hahn et al. 2007; Forero-Romero et al. 2009), the shear of the velocity field (Hoffman et al. 2012; Libeskind et al. 2012, 2013a,b, 2014a), or based on topology of the den-

sity field, e.g., DisPerSE (Sousbie 2011; Sousbie et al. 2011), and so on. In this study, we follow the approach developed by Hahn et al. (2007) and Forero-Romero et al. (2009), which is a dynamical classification scheme of the large scale environment, based on the gravitational potential field of the total matter distribution. Here we present a summary of our implementation of this method.

To characterize the cosmic web and the surrounding large-scale structure of galaxies, we adopt the same mesh setup as we use for the vorticity field calculation (see Section 2.3); in particular, the mesh resolution is compatible to those used in Hahn et al. (2007); Forero-Romero et al. (2009). We first take all particles and assign them to the mesh according to the CIC scheme, yielding the total matter density field ρ_m .

The potential field ϕ_m can then be derived by solving the Poisson’s equation from the matter density field via:

$$\nabla^2 \phi_m = 4\pi G \rho_m. \quad (1)$$

This calculation can be achieved via the Fast Fourier Transform technique. A deformation tensor T_{ij} is then defined as the Hessian of the gravitational potential:

$$T_{ij} \equiv \frac{\partial^2 \phi_m}{\partial x_i \partial x_j}. \quad (2)$$

At each mesh grid point, T_{ij} is calculated using the gradient function with second order accuracy in the PYTHON package NUMPY².

The eigenvalues of T_{ij} , denoted as $\lambda_1, \lambda_2, \lambda_3$ (with $\lambda_1 \geq \lambda_2 \geq \lambda_3$), are then calculated for all grid points. In Hahn et al. (2007), having adopted a threshold value of $\lambda_{\text{th}} = 0$, the authors classified a grid point as knot, filament, sheet, or void according to the number of eigenvalues above λ_{th} . With $\lambda_k > \lambda_{\text{th}}$ ($\lambda_k < \lambda_{\text{th}}$) implying collapse (expansion) along the k th eigenvector, the number of eigenvalues above λ_{th} essentially corresponds to the dimension of the stable manifold at the grid point, specifically, 3 for knot, 2 for filament, 1 for sheet, and 0 for void.

Such a theoretical classification is based on different dynamical nature of large-scale structures. However, it already leads to some marked conflicts when comparing against simulations and the observed Universe even through simple visual inspections. For example, too few voids (only ~ 17 percent in the sense of volume occupation) were classified as shown in Figure 1 of Hahn et al. (2007). Forero-Romero et al. (2009) suggested that this was due to the adoption of a zero threshold, in which case the direction with even infinitesimally positive eigenvalue would be regarded as already “collapse”, causing irrational classifications.

As investigated by Forero-Romero et al. (2009), λ_{th} can be theoretically approximated by equating the free-fall time t_{ff}

² <https://numpy.org>

of the grid to the Hubble time t_H , with $t_{\text{ff}} < t_H$ ($t_{\text{ff}} > t_H$) implying collapse (expansion) of the region. Here we take the theoretical approach to obtain a rough estimate for the threshold value. Using eigenvalues of the deformation tensor and approximating the trace of the deformation tensor with λ_{th} , Eq. (1) can be re-written as:

$$\nabla^2 \phi_m = 4\pi G \rho_m = \lambda_1 + \lambda_2 + \lambda_3 \approx 3\lambda_{\text{th}}. \quad (3)$$

The free-fall time t_{ff} can be expressed using the local density ρ_m of the grid through:

$$t_{\text{ff}} = \sqrt{\frac{3\pi}{32G\rho_m}}. \quad (4)$$

Recalling the Hubble time:

$$t_H = \frac{1}{H_0} \int_0^{+\infty} \frac{dz}{(1+z)E(z)}, \quad (5)$$

where $E(z) = \sqrt{\Omega_m(1+z)^3 + (1-\Omega_m)}$ in a flat universe dominated by matter and dark energy, and z is the redshift. By setting the free-fall time t_{ff} equal to Hubble time t_H and through Eqs. (3), (4) and (5), we then obtain:

$$\lambda_{\text{th}} = \frac{\pi^2 H_0^2}{8} \left(\int_0^{+\infty} \frac{dz}{(1+z)E(z)} \right)^{-2}. \quad (6)$$

In practice through percolation analysis, [Forero-Romero et al. \(2009\)](#) pinned down some effective threshold λ_{th} , which corresponds to $t_{\text{ff}} \approx 2.4t_H$, resulting in reasonable volume fractions for different types of cosmic web structures. In this work, we take one-tenth of the value given by Eq. (6), which yields $t_{\text{ff}} \approx 3t_H$. The volume fractions and one example slice of the four categories are shown in Table 1 and Fig. 1 respectively. This result is consistent with [Martizzi et al. \(2019\)](#), who explored the fractions of different gas phases in four kinds of cosmic structures for the TNG-100 simulation. We note that each central galaxy in the simulation box is then assigned with the corresponding grid type parameters as its large-scale environment type if its centre is located in that grid (i.e. via the *Near Grid Point* algorithm).

In Fig. 2 we present three example slices in the simulation box, each with a thickness of one mesh-cell scale, i.e. ~ 865 kpc. From left to right, the fields are color-coded by the corresponding environment type, total matter vorticity, and cold gas vorticity, respectively. In Section 4, we will present how the cold-gas vorticity depends on the environmental type, as well as the relation between the cold-gas vorticity and central sSFR in different large-scale environments.

3. COLD-GAS VORTICITY ENVIRONMENT AMONG TYPICAL GALAXY SAMPLES

This study is an extension of the previous works ([Wang et al. 2022](#); [Lu et al. 2022b](#)), where we studied the angular momentum modulation of the environment to the CGM

Table 1. The volume fraction of four categories at $z \sim 0$.

Void	Sheet	Filament	Knot
53.75%	33.42%	12.29%	0.54%

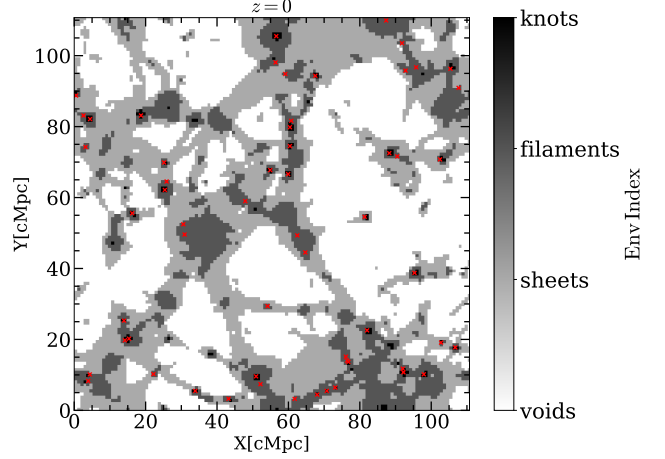


Figure 1. An example slice of the large-scale structure, color-coded by the classified environment type, i.e. voids, sheets, filaments, and knots. The red crosses represent the central galaxies with halo mass larger than $10^{11.5} M_\odot$.

kinematics and star formation activities using about three hundreds typical galaxies from the TNG-100 simulation. As have stated in the introduction, it is the cold gas accretion that is directly relevant to the central star forming activities, we therefore first demonstrate the different motion of the cold gas with respect to the hot component, in the case of the three hundreds galaxies from our previous studies.

These galaxies (within a similar stellar mass range of $10.3 < \log M_*/M_\odot < 11.2$) from our previous studies fall into three categories, i.e., normal star-forming disc galaxies (NMD), dynamically-cold but quenched early-type galaxies (CQ) and dynamically-hot but quenched early-type galaxies (i.e., normal elliptical galaxies, NE). Following Figure 6 in [Lu et al. \(2022b\)](#), here we plot in Fig. 3 the circularity (for definition, see Equation 3 therein) distributions of the CGM gas in the three types of galaxies, but here we split the gas into cold and hot components, same as in [Wang et al. \(2022\)](#), i.e. $T_{\text{gas}} = 10^4 \text{ K} - 2 \times 10^4 \text{ K}$ for the cold and $T_{\text{gas}} > 10^5 \text{ K}$ for the hot. Such a gas circularity defined for each gas cell is essentially the ratio between the specific angular momentum (of this gas cell) projected along the total CGM spin direction (calculated within $5R_{\text{hsm}} < r < 40R_{\text{hsm}}$, where R_{hsm} is the half stellar-mass radius of a galaxy) and the maximum angular momentum of a steady Keplerian orbit at that distance, roughly indicating the strength of rotation. It can be seen that in all three types of galaxies the cold CGM gases always favor higher angular momenta with peaks at $\epsilon > 0.5$ in the

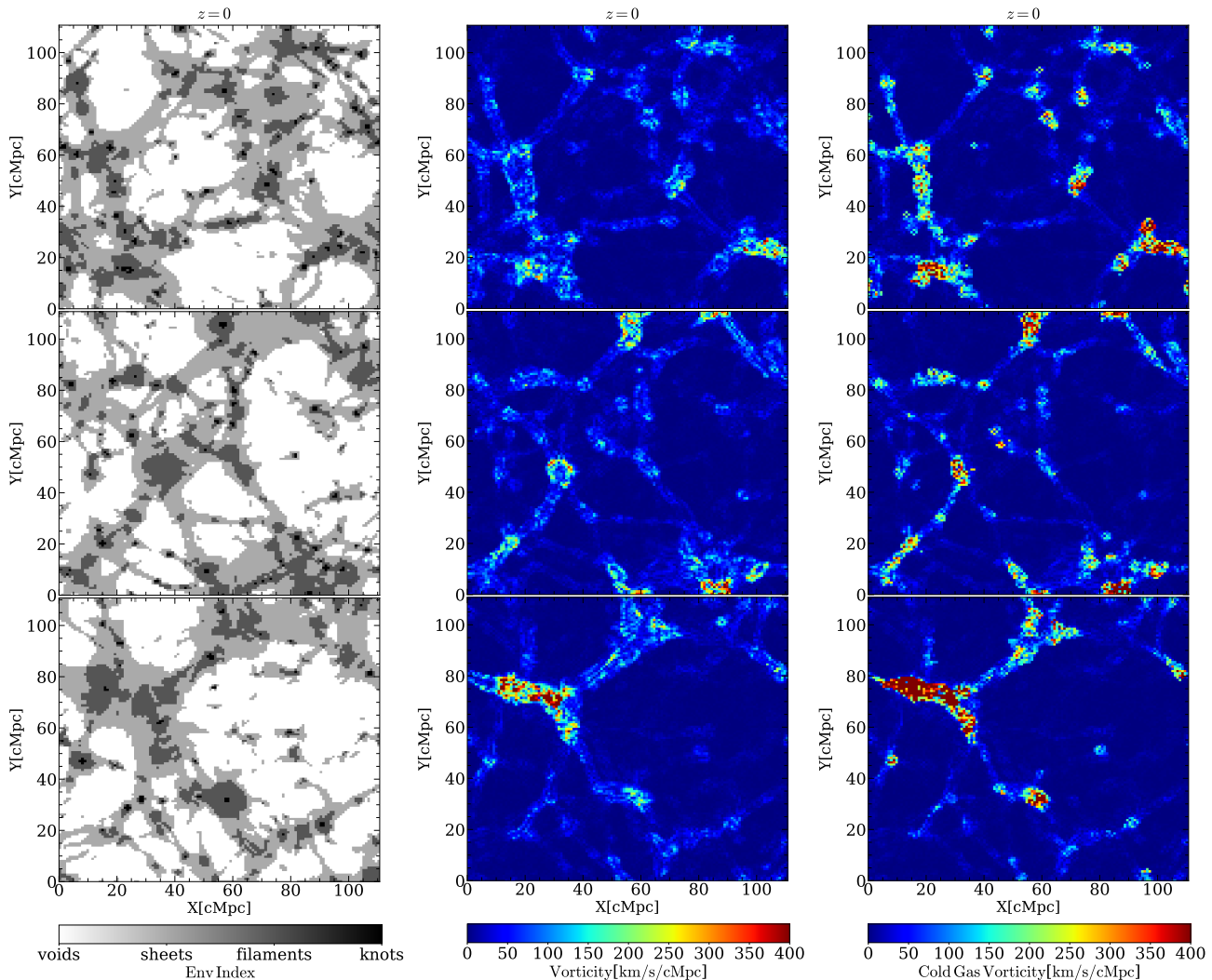


Figure 2. From top to bottom are three example slices of the gridded simulation box, each with a thickness of one mesh-cell scale, i.e. ~ 865 kpc, and from left to right, color-coded by the corresponding environment type, total matter vorticity, and cold gas vorticity, respectively.

gas circularity distributions, in obvious contrast to the hot CGM gases, for which the ϵ distributions peak around zero. The mass fractions of the cold CGM gases that have $\epsilon > 0.5$ are ~ 48 per cent, 68 per cent and 79 per cent for NMDs, NEs and CQs, respectively. The fact that the quenched populations (latter two) generally have larger fractions of their *cold* gas components possessing higher angular momenta in comparison to star-forming galaxies, suggests that the angular/tangential motion possibly prevent cold gas from efficient infalling to smaller radii to fuel central star formation.

The vorticity ω defined as the curl of a velocity field may to some extent indicate the rotational strength of the local matter flow. In Fig. 4, we show the vorticity distributions of the $(\sim 1 \text{ Mpc})^3$ cell environment around the three types of galaxy samples, with the left panel presenting the vorticity of total gas and the right panel the cold gas. It is clear that differences in the cold-gas vorticities among the three galaxy populations are much more significant than those in the to-

tal gas vorticity. In particular, the quenched galaxy samples exhibit much larger cold-gas vorticities than the star-forming samples. Again the star-forming samples live in the environment with lower cold-gas vorticities, conducive to more efficient cold-gas inflow to fuel central star formation, while the opposite is true for the quenched galaxy populations.

4. COLD GAS VORTICITY ENVIRONMENT FOR A GENERAL SAMPLE OF CENTRAL GALAXIES

In this section, we have enlarged the galaxy samples to all central galaxies that have stellar masses with $10.0 < \log M_*/M_\odot < 11.5$, and explored the influence of the large-scale vorticity on galaxy star-formation properties. The lower mass cut is introduced to guarantee sufficient resolution, while the upper mass cut is to, at the sample selection stage, already exclude galaxies whose quenching status can be strongly affected by other mechanisms such as AGN feedbacks. In this section, we mainly focus on the cold-gas vor-

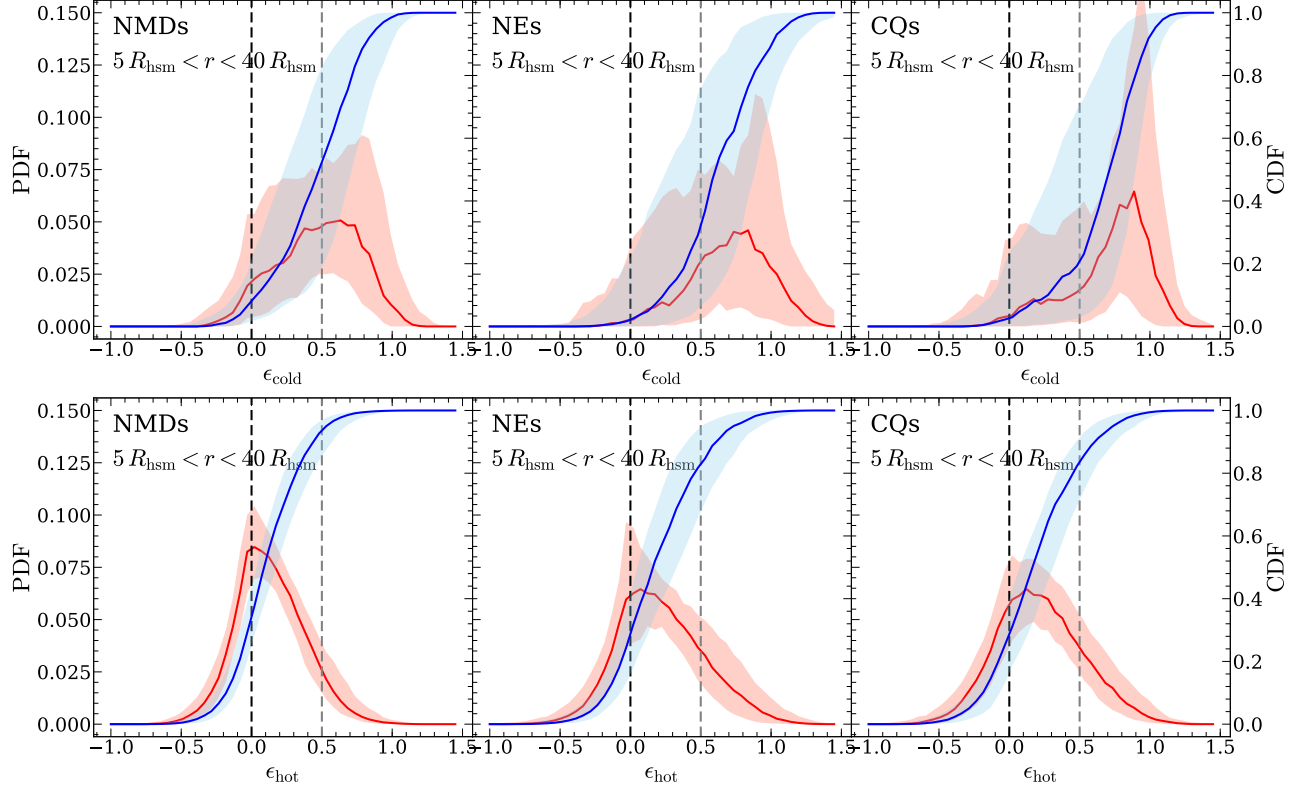


Figure 3. Circularity distributions of the CGM gas among three types of samples at $z \sim 0$ within $5R_{\text{hsm}} < r < 40R_{\text{hsm}}$. The upper row is for the cold CGM and the lower row shows the hot CGM. Red lines represent the probability distribution functions (PDFs) in gas mass and the blue lines are the corresponding cumulative distribution functions (CDFs), with shaded regions indicating the 1σ ranges. Black and grey dashed lines mark the circularity of 0 and 0.5 respectively. The larger the circularity, the closer the gas cell to circular orbit.

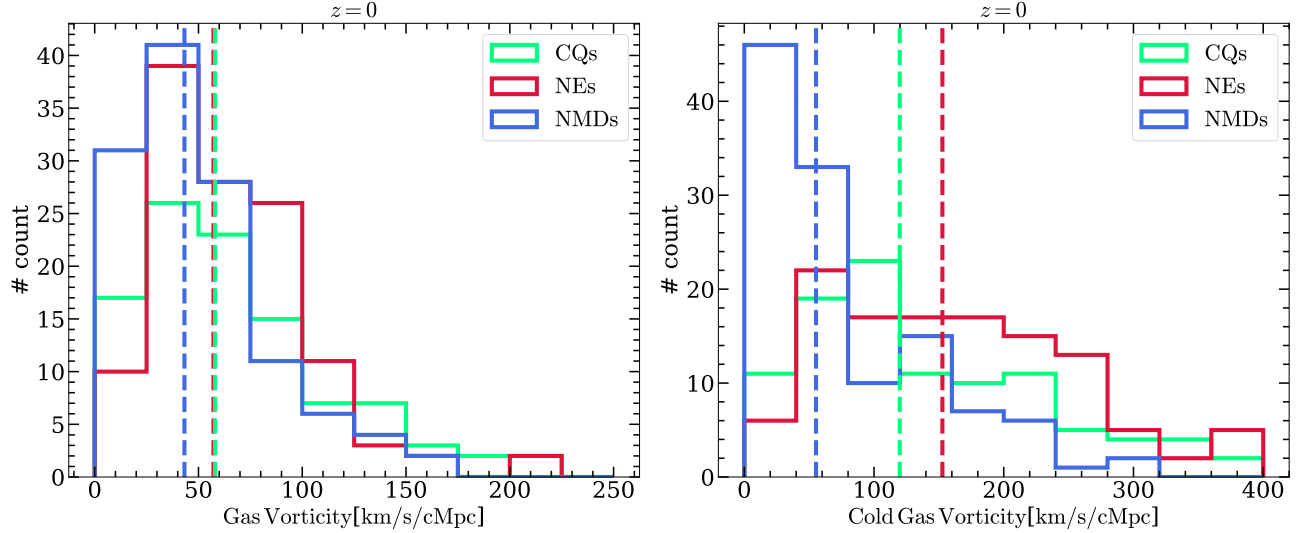


Figure 4. Gas vorticity (left) and cold gas ($T_{\text{gas}} < 2 \times 10^4$ K) vorticity (right) distributions among three types of samples at $z \sim 0$.

ticity properties, because star formation activities are directly related to the cold gas accretion.

4.1. Higher cold-gas vorticity corresponds to lower sSFR

To examine the angular momentum modulation, all central galaxies at $z = 0$ and with stellar masses ranging from $10^{10}M_{\odot}$ to $10^{11.5}M_{\odot}$ are considered. We particularly focus on the comparison between two sub-groups of these galaxies, one among the top 30 per cent and the other among the bottom 30 per cent of a given property. We then examine the distributions of other properties and make comparisons among the two sub-groups. In Fig. 5, the upper left panel shows the cold gas vorticity distributions of galaxies that have the highest (in blue) and the lowest (in red) 30 per cent sSFR (i.e. the most and least star-forming samples). As is shown, statistically more (least) actively star-forming galaxies live in an environment with lower (higher) cold-gas vorticities. When we reverse these two properties and compare the sSFR distributions of the two galaxy samples that live in environments which possess the upper (in red) and lower (in blue) 30 per cent of cold-gas vorticities, as is presented in the lower panel, we also find that the environment that has lower cold-gas vorticities tend to host more actively star-forming galaxies in comparison to its higher vorticity counterpart.

Fig. 5 is necessary to support our angular momentum scenario but not sufficient, because we have not ruled out other factors that might degenerate with the vorticity. For example, we know that both the halo spin and the level of quenching increase with the dark matter halo mass. If the vorticity is also positively correlated with the halo mass, then the suppress of the star formation activity in the high vorticity case could simply because galaxies tend to be more quenched towards higher masses. On the one hand, kinematically, whether the material can flow into the galaxy center or not is partially determined by the strength of the gravitational pull (at given angular momentum). On the other hand, halos with different masses will heat up the CGM to different degrees, resulting in different cooling efficiencies and thus star formation activities. For this reason, we shall also take into account the dependence on halo mass.

Fig. 6 shows the cold gas vorticity (upper panel) and the sSFR (lower panel) as a function of halo mass M_{halo} . We split galaxies into five mass bins, i.e., $\log M_{\text{halo}}/M_{\odot} \in [11.5, 11.9], [11.9, 12.3], [12.3, 12.7], [12.7, 13.1], [13.1, 13.5]$. Within each mass bin, we split the galaxies again into those with the top or bottom 30 per cent of a given property, i.e., either the sSFR or the environmental cold-gas vorticity. The points connected by lines represent the median values of galaxies in the two sub-groups in a given halo mass bin. The error bars represent the $\pm 1\sigma$ scatter. From the upper panel, the trend that the higher (lower) the galaxy sSFR the lower (larger) the cold gas vorticity

is clearly seen across the first three lower-mass bins at below $\log[M_{\text{halo}}/M_{\odot}] \sim 12.7$. However, at the higher mass end above $\log[M_{\text{halo}}/M_{\odot}] \sim 12.7$, the results go opposite. We suspect that, despite of adopting a stellar mass cut at the high mass end, galaxies are still strongly affected by the AGN feedback, which is able to enhance the radial motion of gas kinematics at larger distances, leading to more quenched galaxies (in red) preferably living in a lower vorticity environment. In the lower panel of Fig. 6, we plot the sSFR as a function of halo mass for galaxies that live in environments with upper and lower 30 per cent of the cold-gas vorticity within each mass bin. Again we see that lower (higher) cold gas vorticity environment tends to host more star-forming (quenched) galaxies in the first three lower halo-mass bins. In higher mass bins, although the median values of the two sub-groups exhibit the expected trend, their 1σ scatters are markedly overlapping.

It is worth noting that the negative trend between the cold gas vorticity and the sSFR exhibited here is consistent with the results from our previous studies (Wang et al. 2022; Lu et al. 2022b), where a negative correlation was found between the CGM spin and the sSFR. However, such a correlation can be easily erased or altered, because both the CGM gas motion in the inner parts of halos and the star formation activities can be strongly modulated by various internal feedback effects (as already present here in the highest mass bins). In particular, the trend between the two that we discovered in our previous studies using the TNG-100 simulation could be different using other cosmological simulations which take different approaches to implement feedback processes. In Liu et al. (2024), the authors compared such correlation derived from SIMBA simulation with that from TNG-100 and found totally opposite trend, e.g., quenched galaxies have lower CGM spin. In order to eliminate effects from such internal modulation, we have excluded gases within the central $r_{200}/3$ of each halo (shown in dashed lines) and compared the results with those when including all gases (shown in solid lines). As can be seen, when only taking into account the cold gases at larger distances from halo centres, not only our findings remain present, but also the flip of the trend (in the top panel where the blue and red lines cross) moves to higher mass bins. This indicates that the conclusion on a negative modulation from the (large-scale) cold gas vorticity to galaxy star formation activeness that we report here is not a feature dominated by the interstellar medium or the inner circumgalactic gas, and thus is less susceptible to various internal feedback effects.

4.2. Star-forming versus Quenched

In the former sections, we illustrate the negative impact of high environment angular momentum and high cold gas vorticity to the galaxy star formation activeness. One thing that

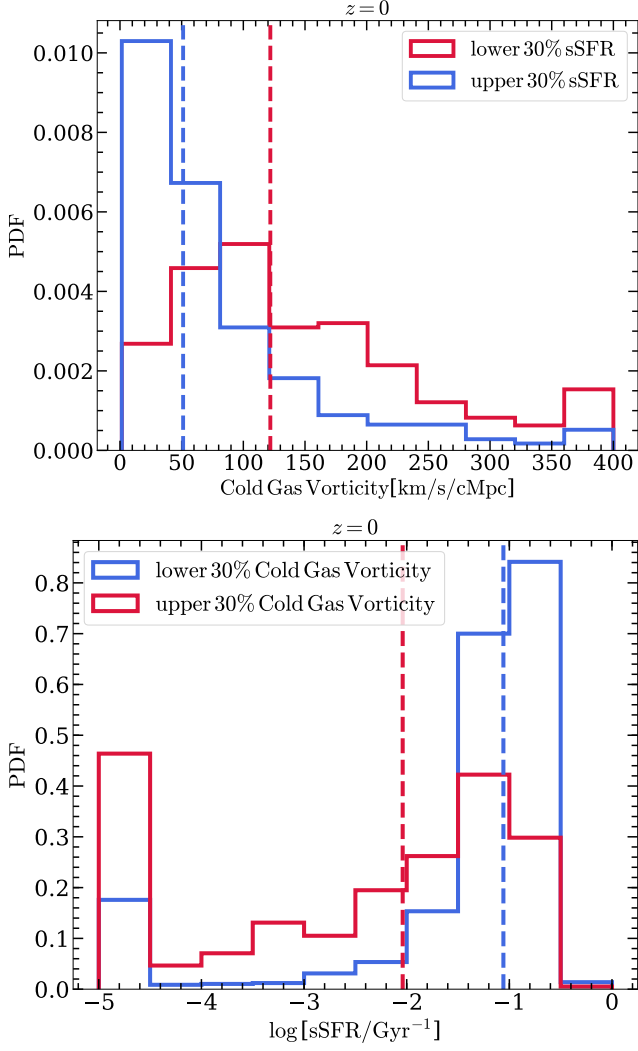


Figure 5. Upper: The cold gas vorticity distributions of galaxies with top (blue) and bottom (red) 30 per cent sSFR. Lower: The sSFR distributions of galaxies with top (red) and bottom (blue) cold gas vorticity. All sample galaxies are centrals with stellar mass in $10^{10}M_{\odot} - 10^{11.5}M_{\odot}$ at $z \sim 0$.

we shall emphasize is that we do not propose this mechanism to account for the significant shutdown of the past star formation in present-day quenched galaxies. For these galaxies, the angular momentum mechanism only serves in the “post-quenched” phase, playing a role of preventing the system from efficient cold-gas supplement to galaxy centres and thus further star formation, when the environmental angular momentum is high. In fact, if it is otherwise, i.e., the environmental gas angular momentum is not sufficiently high, then galaxies might rejuvenate, moving back to the blue cloud from the green valley (or even the red sequence), back and forth, experiencing episodic star formation history, either before a complete shutdown of star formation in present-day quenched galaxies (e.g., Tacchella et al. 2016; Behroozi et al.

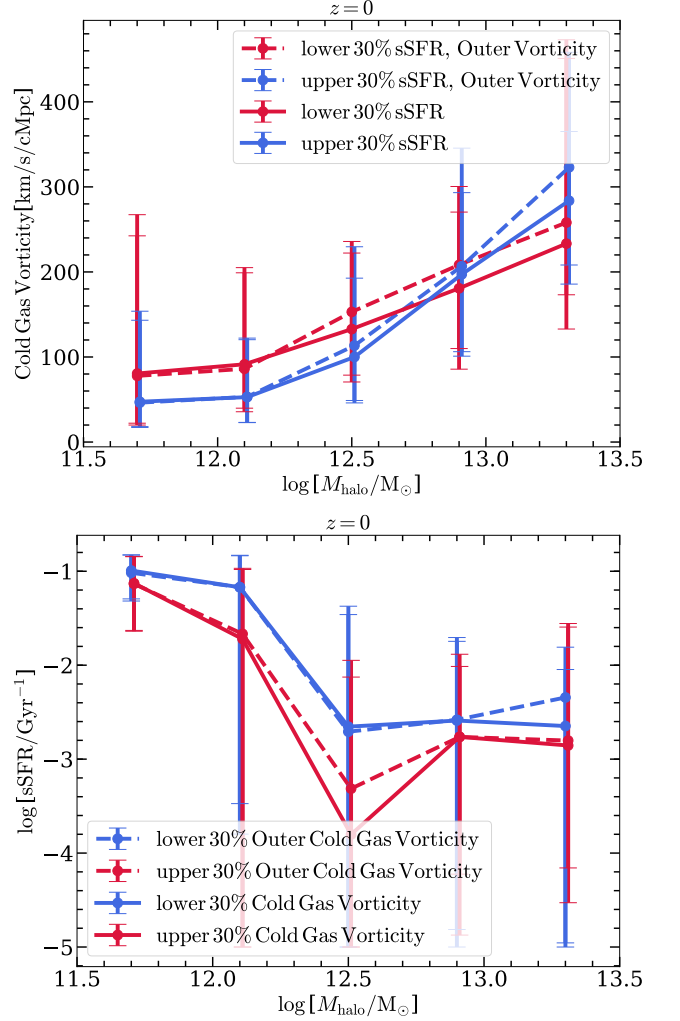


Figure 6. Upper: The cold gas vorticity distributions of galaxies with top (blue) and bottom (red) 30 per cent sSFR in each halo mass bin. Lower: The sSFR distributions of galaxies with top (red) and bottom (blue) 30 per cent cold gas vorticity in each halo mass bin. Data points show the median values and errorbars are the 1σ scales. Solid and dashed lines represent the results for vorticity of all cold gas and cold gas excluding any halo’s central part, i.e. $1/3 r_{200}$.

2019; Wang et al. 2019), or throughout the late-time evolution of present-day star-forming galaxies (see Figure 1 of Wang et al. 2022).

A further clarification is that the angular momentum mechanism does not only takes effect after galaxies being quenched. The low/high angular momentum environment is always there and universally affects the gas acquisition efficiency and thus SFR for all types of galaxies, also including star-forming galaxies. To demonstrate this, we dichotomously divide galaxies into star-forming and quenched samples, as separated by $\log[\text{sSFR}/\text{Gyr}^{-1}] = -2.0$ (e.g., Lu et al. 2022a). For either galaxy population, we plot the

sSFR distribution as a function of halo mass, as is shown in Fig. 7, and make comparisons between the two sub-groups of galaxies that live in the top and bottom 30 per cent cold-vorticity environments within each halo mass bin. We note that in the right panels of Fig. 7 (i.e., for quenched galaxies), we have dismissed galaxies that are totally quenched (i.e. $\log[\text{sSFR}/\text{Gyr}^{-1}] \leq -5$) in order to reduce the contamination due to the much stronger quenched mechanisms related to baryonic feedback processes. As can be seen, for either galaxy population and within each halo mass bin, galaxies that live in environments with larger (smaller) cold-gas vorticities (as presented in the top panels) always tend to have lower (higher) sSFR (as shown in the bottom panels). It is clear that a negative modulation of angular momentum to star formation activeness has been widely observed among both star-forming and quenched galaxy populations.

4.3. Dependence on Larger-Scale Environment Type

As already introduced in Section 1, past studies already revealed that the angular momentum environment, in particular the vortical flow associated with different large-scale environments acts on different levels. In this work, we have also investigated how the environmental cold-gas vorticity and its influence on galaxy star formation would differ among different large-scale environmental types. In particular, we make comparisons between situations in filaments and knots.

Fig. 8 shows the cold gas vorticity distribution as a function of halo mass for galaxies living in filaments (in blue) and in knots (in red). In either case, again we select two galaxy sub-groups, i.e., the ones with upper (dashed line) and lower (solid line) 30 per cent sSFR, within each halo mass bin. As can be seen, filaments generally host less massive halos (typically below $\log[M_{\text{halo}}/M_{\odot}] \sim 12.7$) than knots, this is because frequent mergers happen to knot galaxies, boosting the growing of their halo masses. At a fixed halo mass, galaxies living in filaments in general exhibit higher environmental cold-gas vorticities than those living in knots. We attribute this to the rich dynamics of the cosmic web structure (see e.g., Pichon et al. 2011). At below $\log[M_{\text{halo}}/M_{\odot}] \sim 12.7$ (i.e., in the first three mass bins), for galaxies in both types of environments, the sub-groups with lower (upper) 30 per cent sSFR live in an environment that has higher (lower) cold-gas vorticities, again revealing a negative modulation of the angular momentum environment to the central star formation. At the higher halo end, knot galaxies dominate the population and exhibit the opposite trend (a similar result is also presented in Fig. 6). We again attribute this to the correlation between the lower sSFR of galaxies and the strong AGN feedback possibly causing a lower vorticity environment.

We then select galaxy sub-groups according to their environmental cold gas vorticities (upper and lower 30 per cent) within each halo mass bin and for a given environmental

type. The median sSFR are then compared between the two subgroups at any given halo mass. The results in the filament and knot environments are shown in the left and right panels of Fig. 9, respectively. The negative correspondence between higher (lower) environmental cold-gas vorticities and lower (higher) sSFR is again revealed by the dashed (solid) lines. It also can be seen that the upper (and lower) 30 per cent cold gas vorticities of the filament environment are systematically higher than that of the knot environment (comparing the left- and right-hand sides in the upper panels). This naturally explains the comparisons in sSFR between galaxies from the two environmental types, in that filament galaxies have systematically lower sSFR than the knot galaxies for any given halo mass, as presented in the lower panels of the figure.

5. DISCUSSION

5.1. In Relation to Orbital Angular Momentum of Galaxy Neighborhood

In Lu et al. (2022b), the authors found a positive correlation between the orbital angular momentum of environmental galaxies and the cold CGM spin of the central galaxy (see Figure 4 and Figure 9 therein), evidencing an external angular momentum modulation of the environment (from satellite galaxies) to the cold circumgalactic gas (as is also clearly evident from Figure 7 and 8 in Wang et al. 2022). As this is a natural consequence of gas acquisition within the context of galaxy merger and interaction, such a positive correlation shall be universally present across different simulations, although the negative correlation between the CGM spin and galaxy sSFR may or may not exist. This is indeed the case as reported by Liu et al. (2024), where the positive correlation was also discovered using the SIMBA simulation.

Here we extend such investigation into the cosmic environment on larger scales and search for correlations between a galaxy's environmental cold gas vorticity and the orbital (specific) angular momentum from its close neighborhood. For the latter calculation, we take all satellite galaxies within a radial distance range from 30 kpc to 500 kpc from any given central galaxy. The results are presented in Fig. 10. As can be seen from the top panel, galaxies that live in environments with upper (lower) 30 per cent cold-gas vorticities also exhibit higher (lower) orbital angular momenta at any given halo mass. In the bottom panel, we reverse the two properties in the plot. It can also be seen that galaxies that possess upper (lower) 30 per cent orbital angular momenta also live in environments that show higher (lower) cold-gas vorticities.

It is worth noting that both the cold gas on larger scales and neighboring galaxies moving along the same cosmic web structure, are tracers of the larger-scale gravitational field. Their angular momentum properties are both essentially inherited from the tidal torque field established by the large-scale structure and later on affected by the rich and non-linear

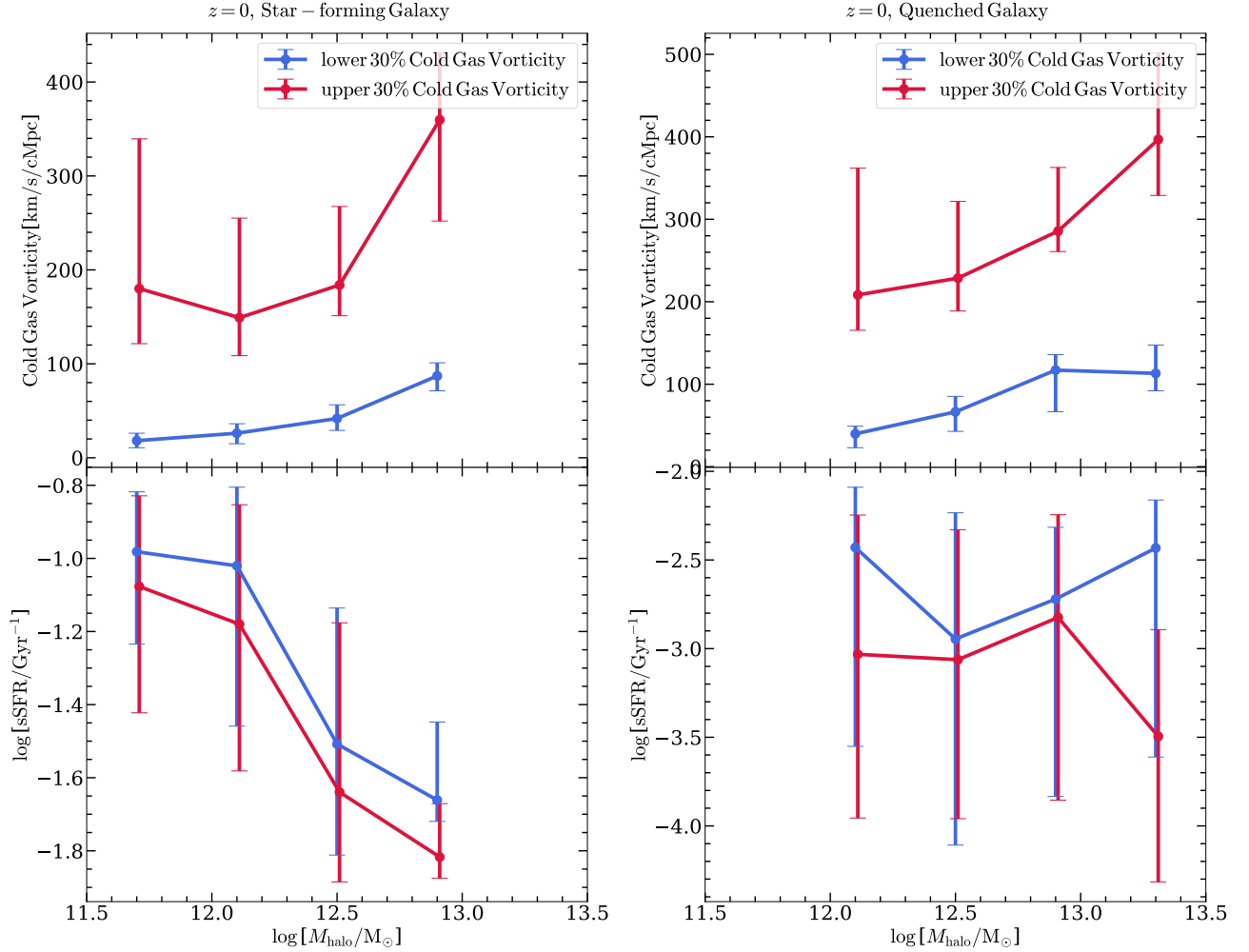


Figure 7. Cold gas vorticity (top) and sSFR (bottom) distributions of samples with top 30 per cent (red) and bottom 30 per cent (blue) cold gas vorticity in each halo mass bin. Left panels are for star-forming galaxies and right ones are quenched samples. Galaxies that are totally quenched, i.e. with $\log[\text{sSFR}/\text{Gyr}^{-1}] \leq -5$, are ignored here.

dynamics of matter accretion along the cosmic web. However, as will be shown in the next subsection, the cold gas component, being a highly collisional and dissipational matter component, behaves very differently in terms of its vorticity field, from the dark matter as well as the total gas species (which is largely dominated by the hot gas component on large scales around galaxies). In particular, as demonstrated in Wang et al. (2022), the kinetic motion of the cold circumgalactic gas can be significantly affected by galaxy interactions such as mergers and fly-bys (see Figure 7 and 8 therein). Here we also expect that galaxy interactions may strongly affect the cold-gas vorticity field, transferring angular momentum at distances of several hundreds of kpc and even beyond.

These findings also suggest that future observational efforts towards measuring the two environmental angular momentum properties, and seeking for correlations between themselves, as well as between them and galaxy properties

(such as SFR, stellar size, angular momentum, and kinematics), would provide key information for us to better understand the co-evolution between galaxies and their larger-scale environment. In particular, we propose two kinds of galaxies and their larger-scale environments as ideal test sites, i.e., superthin galaxies and low surface brightness galaxies. Theoretical studies based on cosmological simulations revealed tight correlations between their large angular momenta and large disk length-to-height ratios (Hu et al. 2024), and between their large angular momenta and their larger sizes and thus low surface brightnesses (see Pérez-Montaño et al. 2022, 2024; Zhu et al. 2023). Both kinds of galaxies tend to live in more isolated environments, and therefore their stellar angular momenta manage to better retain angular momenta of the accreted cold gas, which are greatly modulated by the larger-scale galaxy interaction environment. We predict that these galaxies must preferably live in environments with higher cold-gas vorticities, which also exhibit more strongly co-

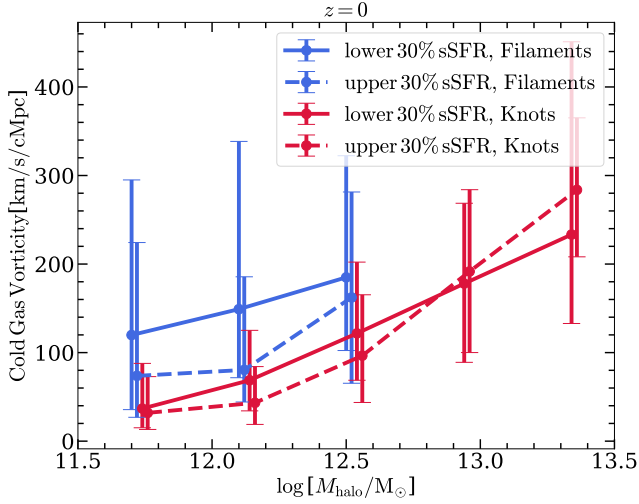


Figure 8. The cold gas vorticity distributions of galaxies in filaments (blue) and knots (red). In both environments, galaxies with top (dashed lines) and bottom (solid lines) 30 per cent sSFR in each halo mass bin are selected.

herent kinematic motions among neighboring galaxies, the CGM, and the central stellar disks across a wide distance scales (see Figure 9 of Lu et al. 2022b).

5.2. Vorticities in total matter, total gas and cold gas

As already discussed, different matter species within and around galaxy halos receive different angular momenta via different modulation mechanisms. It is therefore expected to observe different angular momenta between the dark matter, gas and stellar components. The same is also true here in the case of the matter vorticity fields. In this section, we present the difference between the environmental vorticity fields of the total matter, the total gas component, and the cold gas component. As will be seen, the last always exhibits the highest vorticities in the same region, due to its unique, highly collisional and dissipational nature.

This can be clearly seen from Fig. 2, where the magnitudes of the cold-gas vorticity fields are significantly larger than those of the total matter vorticity fields. The same trend is also evident in Fig. 11, where we plot the field strengths of three types of vorticities, i.e., the total matter (left-most), the total gas (middle), and the cold gas (right-most), as a function of the field over-density. In this figure, only grid cells with a total stellar masses (from central galaxies) larger than $10^{10}M_{\odot}$ are used. Each panel is also color-coded by the grid sSFR (averaged within a region of ~ 1 Mpc). As the matter over-density increases (horizontally from left to right), the region average sSFR decreases - a result widely confirmed by previous studies (e.g., Winkel et al. 2021; Galárraga-Espinosa et al. 2023; Hasan et al. 2023, 2024). It can also be seen that, as the cold-gas vorticity increases (vertically from bottom to top), the sSFR also decrease significantly

(the right-most panel, and also presented in Section 4). This trend, however, only exists for the cold-gas vorticity, but neither in the case of total matter vorticity, nor the total gas vorticity. As discussed already, this is a result of the uniqueness of cold gas, which can cool efficiently while gravitationally influenced by the cosmic web structure, forming highly localized vortical flow, in comparison to its hotter-gas or dark matter counterparts.

6. CONCLUSIONS

In this study, we take the TNG-100 simulation and investigate the influence of the large-scale angular momentum environment as depicted by a cold-gas vorticity, on a galaxy’s star formation activeness depicted by sSFR. This vorticity calculated for gas with $T_{\text{gas}} < 2 \times 10^4 \text{K}$ and on scales of ~ 1 Mpc can well describe the angular motion of the ambient cold gas. We find crucial evidence for a clear connection between the cold gas spin/vorticity and star formation activeness, in that for any given halo mass, galaxies that live in a higher cold-gas vorticity environment are generally less actively star forming (Section 4.1). This is true among both star-forming and quenched galaxy populations (Section 4.2). This environmental cold-gas vorticity also varies with different large-scale environment types. At any fixed halo mass scale, the environmental cold-gas vorticities in filaments are generally higher than that in knots, naturally explaining lower sSFRs in filament galaxies than in knot galaxies (Section 4.3). We find that this quantity, as expected, is highly connected to the orbital angular momentum of neighbouring galaxies, indicating their common origins and possible interplay with each other (Section 5.1). It is also worth noting that such a negative modulation by the environmental vorticity to galaxy star formation is only significantly observed for the cold gas, but not for either the total matter or the total gas component (Section 5.2), indicating the unique role of cold gas. We emphasize that the angular/vortical motion on large scales, as manifested through the vorticity field, in particular that associated with the cold gas, is a crucial element shaping the star-forming and quenching status of a galaxy, and thus an important feature, among others, to depict a galaxy’s larger-scale environment, when studying the co-evolution between the galaxies and their large-scale environments.

Finally we also stress that the negative modulation between the angular momentum environment and galaxy star formation as reported here is markedly evident in the TNG simulation. However, this might not be the case in other cosmological simulations which take on different sub-grid models to treat feedback (e.g., Liu et al. 2024). One obvious reason is that for a causal connection between the large-scale cold-gas angular momentum environment and the central star-formation activity to exist, there shall be a crucial mechanism that can effectively transfer the large-scale CGM angular mo-

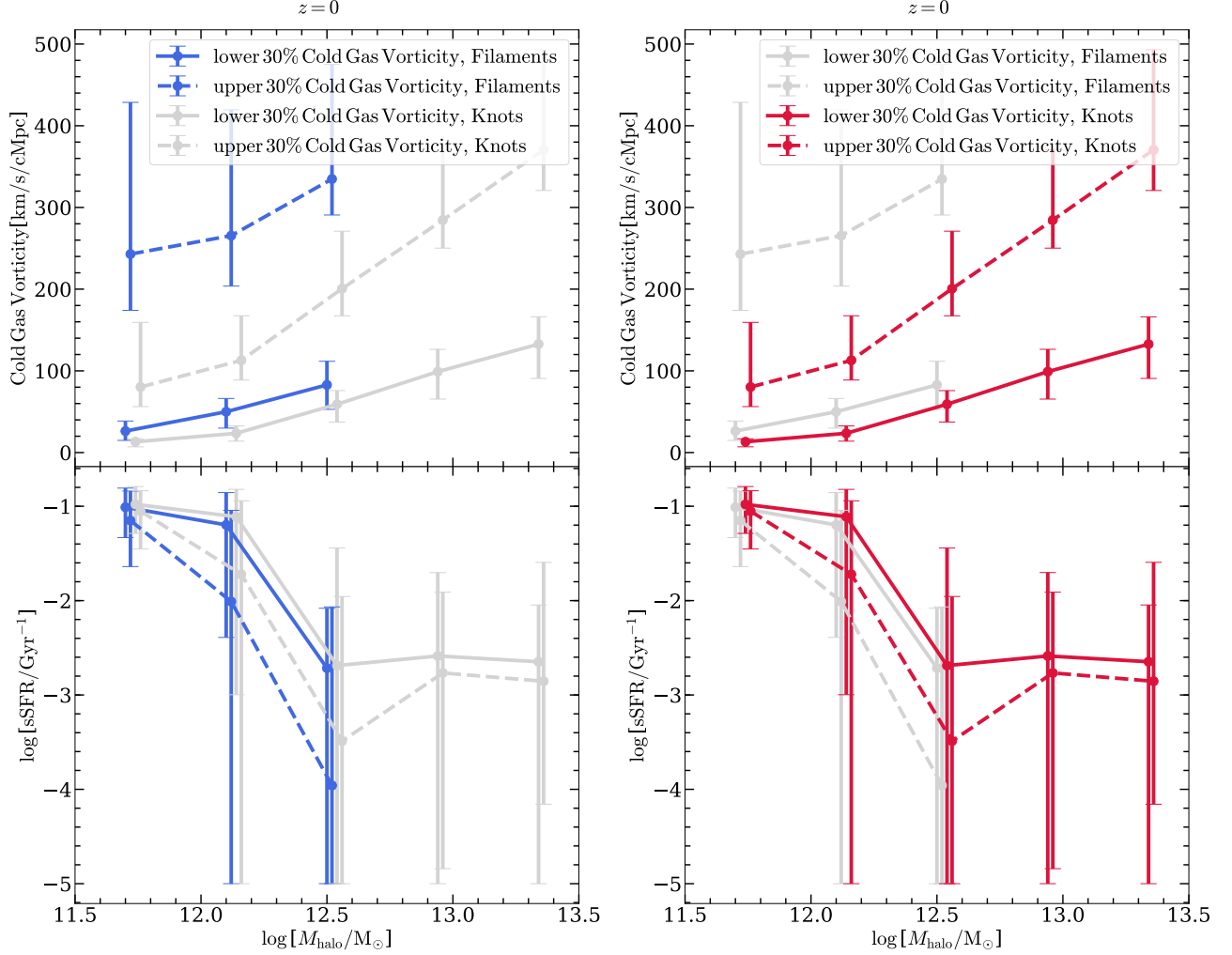


Figure 9. Upper: Similar to Fig. 7, top and bottom panels show the galaxy cold gas vorticity and sSFR distributions respectively. Samples are also divided according to environment type, with blue lines for filament galaxies and red ones for knot galaxies. Dashed lines represent the results of galaxies with top 30 per cent cold gas vorticity in each halo mass bin while solid lines are for galaxies with bottom 30 per cent cold gas vorticity. For visual convenience, we shade the knot (filament) data in left (right) panel.

ment to the ISM through mixing, which strongly depends on the detailed sub-grid models for the ISM feedback. A recent study by Yang et al. (2024) compared between the Apostle (Sawala et al. 2016; Fattahi et al. 2016) and Auriga (Grand et al. 2017) simulations and clearly demonstrated so. It is therefore worth examining such signals using other cosmological simulations of the kind.

ACKNOWLEDGEMENTS

We acknowledge Drs. Volker Springel and Simon White for their constructive suggestions which help to better deliver the key idea of the study. We also thank Prof. Cheng Li for his helpful advice. This work is supported by the National Key Research Development Program of China (Grant No. 2022YFA1602903) and the National Natural Science Foundation of China (Grant No. 12433003). This work acknowledges the high-performance computing clusters at the Department of Astronomy, Tsinghua University.

REFERENCES

Barnes, J., & Efstathiou, G. 1987, *ApJ*, 319, 575,

Behroozi, P., Wechsler, R. H., Hearin, A. P., & Conroy, C. 2019,

doi: [10.1086/165480](https://doi.org/10.1086/165480)

MNRAS, 488, 3143, doi: [10.1093/mnras/stz1182](https://doi.org/10.1093/mnras/stz1182)

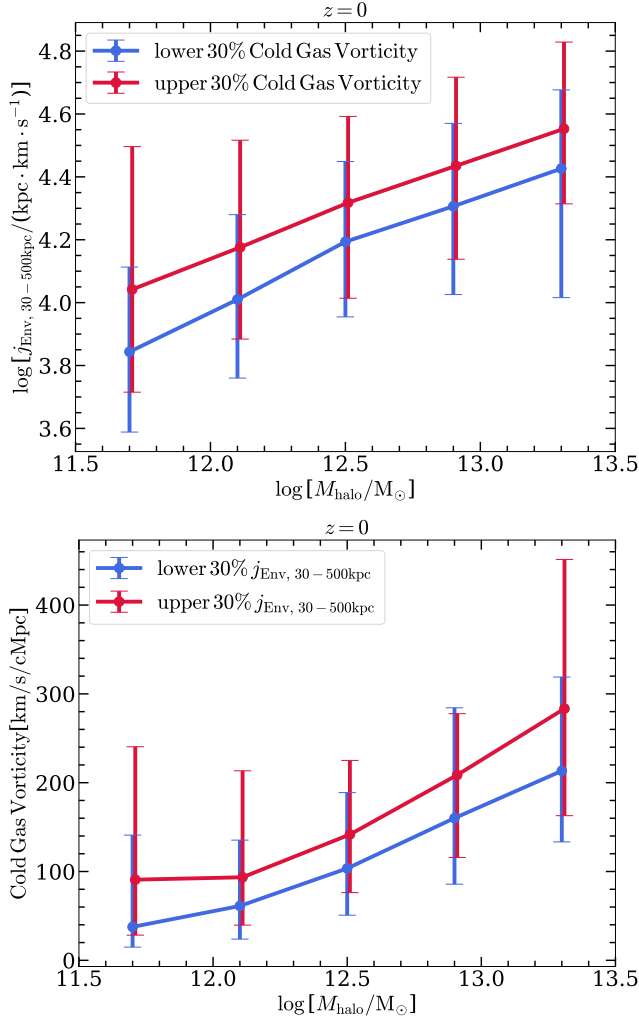


Figure 10. Upper: The environmental satellite orbital angular momentum distributions of galaxies with top (red) and bottom (blue) 30 per cent cold gas vorticity in each halo mass bin. Lower: The cold gas vorticity distributions of galaxies with the top (red) and bottom (blue) 30 per cent satellite orbital angular momentum in each halo mass bin.

Bernardeau, F., Colombi, S., Gaztañaga, E., & Scoccimarro, R. 2002, *PhR*, 367, 1, doi: [10.1016/S0370-1573\(02\)00135-7](https://doi.org/10.1016/S0370-1573(02)00135-7)

Bett, P., Eke, V., Frenk, C. S., et al. 2007, *MNRAS*, 376, 215, doi: [10.1111/j.1365-2966.2007.11432.x](https://doi.org/10.1111/j.1365-2966.2007.11432.x)

Bett, P., Eke, V., Frenk, C. S., Jenkins, A., & Okamoto, T. 2010, *MNRAS*, 404, 1137, doi: [10.1111/j.1365-2966.2010.16368.x](https://doi.org/10.1111/j.1365-2966.2010.16368.x)

Bett, P. E., & Frenk, C. S. 2016, *MNRAS*, 461, 1338, doi: [10.1093/mnras/stw1395](https://doi.org/10.1093/mnras/stw1395)

Bois, M., Emsellem, E., Bournaud, F., et al. 2011, *MNRAS*, 416, 1654, doi: [10.1111/j.1365-2966.2011.19113.x](https://doi.org/10.1111/j.1365-2966.2011.19113.x)

Bullock, J. S., Dekel, A., Kolatt, T. S., et al. 2001, *ApJ*, 555, 240, doi: [10.1086/321477](https://doi.org/10.1086/321477)

Catelan, P., & Theuns, T. 1996, *MNRAS*, 282, 455, doi: [10.1093/mnras/282.2.455](https://doi.org/10.1093/mnras/282.2.455)

Cattaneo, A., Faber, S. M., Binney, J., et al. 2009, *Nature*, 460, 213, doi: [10.1038/nature08135](https://doi.org/10.1038/nature08135)

Codis, S., Pichon, C., Devriendt, J., et al. 2012, *MNRAS*, 427, 3320, doi: [10.1111/j.1365-2966.2012.21636.x](https://doi.org/10.1111/j.1365-2966.2012.21636.x)

Cortese, L., Fogarty, L. M. R., Bekki, K., et al. 2016, *MNRAS*, 463, 170, doi: [10.1093/mnras/stw1891](https://doi.org/10.1093/mnras/stw1891)

Croton, D. J., Springel, V., White, S. D. M., et al. 2006, *MNRAS*, 365, 11, doi: [10.1111/j.1365-2966.2005.09675.x](https://doi.org/10.1111/j.1365-2966.2005.09675.x)

Danovich, M., Dekel, A., Hahn, O., Ceverino, D., & Primack, J. 2015, *MNRAS*, 449, 2087, doi: [10.1093/mnras/stv270](https://doi.org/10.1093/mnras/stv270)

Danovich, M., Dekel, A., Hahn, O., & Teyssier, R. 2012, *MNRAS*, 422, 1732, doi: [10.1111/j.1365-2966.2012.20751.x](https://doi.org/10.1111/j.1365-2966.2012.20751.x)

DeFelippis, D., Genel, S., Bryan, G. L., & Fall, S. M. 2017, *ApJ*, 841, 16, doi: [10.3847/1538-4357/aa6dfc](https://doi.org/10.3847/1538-4357/aa6dfc)

Di Matteo, T., Colberg, J., Springel, V., Hernquist, L., & Sijacki, D. 2008, *ApJ*, 676, 33, doi: [10.1086/524921](https://doi.org/10.1086/524921)

Di Matteo, T., Springel, V., & Hernquist, L. 2005, *Nature*, 433, 604, doi: [10.1038/nature03335](https://doi.org/10.1038/nature03335)

Dolag, K., Borgani, S., Murante, G., & Springel, V. 2009, *MNRAS*, 399, 497, doi: [10.1111/j.1365-2966.2009.15034.x](https://doi.org/10.1111/j.1365-2966.2009.15034.x)

Doroshkevich, A. G. 1970, *Astrophysics*, 6, 320, doi: [10.1007/BF01001625](https://doi.org/10.1007/BF01001625)

Efstathiou, G., & Silk, J. 1983, *FCPh*, 9, 1

Emsellem, E., Cappellari, M., Krajnović, D., et al. 2011, *MNRAS*, 414, 888, doi: [10.1111/j.1365-2966.2011.18496.x](https://doi.org/10.1111/j.1365-2966.2011.18496.x)

Fall, S. M., & Efstathiou, G. 1980, *MNRAS*, 193, 189, doi: [10.1093/mnras/193.2.189](https://doi.org/10.1093/mnras/193.2.189)

Fattahi, A., Navarro, J. F., Sawala, T., et al. 2016, *MNRAS*, 457, 844, doi: [10.1093/mnras/stv2970](https://doi.org/10.1093/mnras/stv2970)

Firmani, C., & Avila-Reese, V. 2000, *MNRAS*, 315, 457, doi: [10.1046/j.1365-8711.2000.03338.x](https://doi.org/10.1046/j.1365-8711.2000.03338.x)

—. 2009, *MNRAS*, 396, 1675, doi: [10.1111/j.1365-2966.2009.14844.x](https://doi.org/10.1111/j.1365-2966.2009.14844.x)

Forero-Romero, J. E., Hoffman, Y., Gottlöber, S., Klypin, A., & Yepes, G. 2009, *MNRAS*, 396, 1815, doi: [10.1111/j.1365-2966.2009.14885.x](https://doi.org/10.1111/j.1365-2966.2009.14885.x)

Galárraga-Espinosa, D., Garaldi, E., & Kauffmann, G. 2023, *A&A*, 671, A160, doi: [10.1051/0004-6361/202244935](https://doi.org/10.1051/0004-6361/202244935)

Gómez-Marín, M., Santos-Santos, I., Domínguez-Tenreiro, R., et al. 2024, *ApJ*, 965, 154, doi: [10.3847/1538-4357/ad27da](https://doi.org/10.3847/1538-4357/ad27da)

Genel, S., Fall, S. M., Hernquist, L., et al. 2015, *ApJL*, 804, L40, doi: [10.1088/2041-8205/804/2/L40](https://doi.org/10.1088/2041-8205/804/2/L40)

Gott, J. R., I. 1977, *ARA&A*, 15, 235, doi: [10.1146/annurev.aa.15.090177.001315](https://doi.org/10.1146/annurev.aa.15.090177.001315)

Granato, G. L., De Zotti, G., Silva, L., Bressan, A., & Danese, L. 2004, *ApJ*, 600, 580, doi: [10.1086/379875](https://doi.org/10.1086/379875)

Grand, R. J. J., Gómez, F. A., Marinacci, F., et al. 2017, *MNRAS*, 467, 179, doi: [10.1093/mnras/stx071](https://doi.org/10.1093/mnras/stx071)

Hahn, O., Angulo, R. E., & Abel, T. 2015, *MNRAS*, 454, 3920, doi: [10.1093/mnras/stv2179](https://doi.org/10.1093/mnras/stv2179)

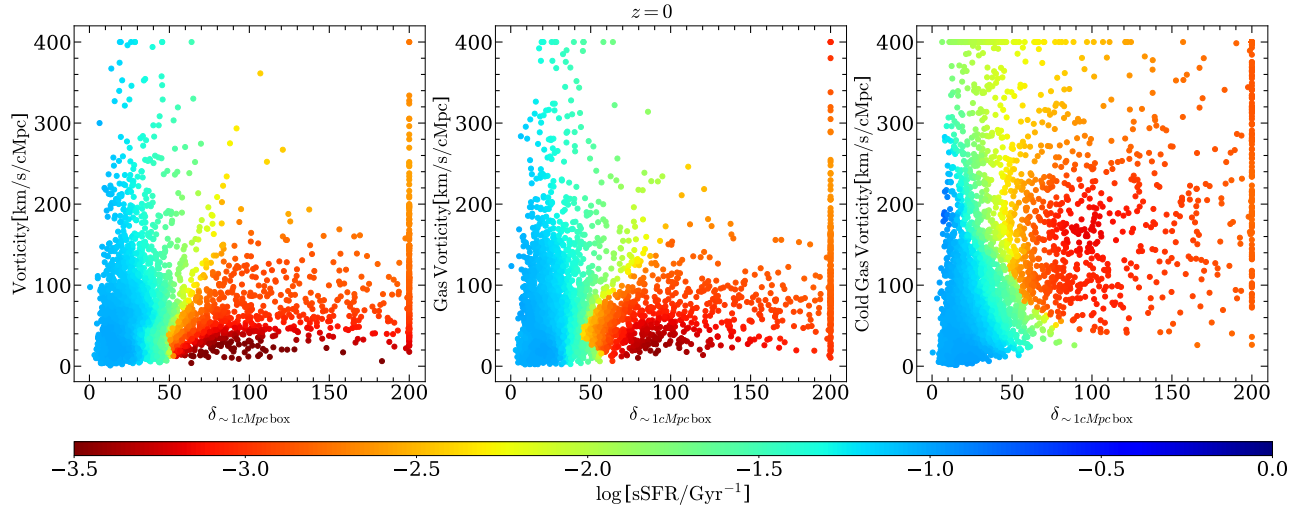


Figure 11. Distributions of grid cells (with total stellar mass from *central* galaxies larger than $10^{10}M_{\odot}$) on the over-density – vorticity phase space, color-coded by the *cell* specific SFR at $z = 0$. From left to right, the y -axis denotes the vorticity of the total matter, total gas, and the cold gas, respectively.

- Hahn, O., Porciani, C., Carollo, C. M., & Dekel, A. 2007, MNRAS, 375, 489, doi: [10.1111/j.1365-2966.2006.11318.x](https://doi.org/10.1111/j.1365-2966.2006.11318.x)
- Hasan, F., Burchett, J. N., Abeyta, A., et al. 2023, ApJ, 950, 114, doi: [10.3847/1538-4357/acd11c](https://doi.org/10.3847/1538-4357/acd11c)
- Hasan, F., Burchett, J. N., Hellinger, D., et al. 2024, ApJ, 970, 177, doi: [10.3847/1538-4357/ad4ee2](https://doi.org/10.3847/1538-4357/ad4ee2)
- Hetznecker, H., & Burkert, A. 2006, MNRAS, 370, 1905, doi: [10.1111/j.1365-2966.2006.10616.x](https://doi.org/10.1111/j.1365-2966.2006.10616.x)
- Ho, S. H., Martin, C. L., Kacprzak, G. G., & Churchill, C. W. 2017, ApJ, 835, 267, doi: [10.3847/1538-4357/835/2/267](https://doi.org/10.3847/1538-4357/835/2/267)
- Hoffman, Y., Metuki, O., Yepes, G., et al. 2012, MNRAS, 425, 2049, doi: [10.1111/j.1365-2966.2012.21553.x](https://doi.org/10.1111/j.1365-2966.2012.21553.x)
- Hopkins, P. F., Hernquist, L., Cox, T. J., et al. 2005, ApJ, 630, 705, doi: [10.1086/432438](https://doi.org/10.1086/432438)
- Hu, J., Xu, D., & Li, C. 2024, Research in Astronomy and Astrophysics, 24, 075019, doi: [10.1088/1674-4527/ad5399](https://doi.org/10.1088/1674-4527/ad5399)
- Jones, B. J. T. 1976, Reviews of Modern Physics, 48, 107, doi: [10.1103/RevModPhys.48.107](https://doi.org/10.1103/RevModPhys.48.107)
- Laigle, C., Pichon, C., Codis, S., et al. 2015, MNRAS, 446, 2744, doi: [10.1093/mnras/stu2289](https://doi.org/10.1093/mnras/stu2289)
- Liao, S., Gao, L., Frenk, C. S., Guo, Q., & Wang, J. 2017, MNRAS, 470, 2262, doi: [10.1093/mnras/stx1391](https://doi.org/10.1093/mnras/stx1391)
- Libeskind, N. I., Hoffman, Y., Forero-Romero, J., et al. 2013a, MNRAS, 428, 2489, doi: [10.1093/mnras/sts216](https://doi.org/10.1093/mnras/sts216)
- Libeskind, N. I., Hoffman, Y., & Gottlöber, S. 2014a, MNRAS, 441, 1974, doi: [10.1093/mnras/stu629](https://doi.org/10.1093/mnras/stu629)
- Libeskind, N. I., Hoffman, Y., Knebe, A., et al. 2012, MNRAS, 421, L137, doi: [10.1111/j.1745-3933.2012.01222.x](https://doi.org/10.1111/j.1745-3933.2012.01222.x)
- Libeskind, N. I., Hoffman, Y., Steinmetz, M., et al. 2013b, ApJL, 766, L15, doi: [10.1088/2041-8205/766/2/L15](https://doi.org/10.1088/2041-8205/766/2/L15)
- Libeskind, N. I., Knebe, A., Hoffman, Y., & Gottlöber, S. 2014b, MNRAS, 443, 1274, doi: [10.1093/mnras/stu1216](https://doi.org/10.1093/mnras/stu1216)
- Liu, K., Guo, H., Wang, S., et al. 2024, arXiv e-prints, arXiv:2409.09379, doi: [10.48550/arXiv.2409.09379](https://doi.org/10.48550/arXiv.2409.09379)
- Lu, S., Xu, D., Wang, S., et al. 2022a, MNRAS, 509, 5062, doi: [10.1093/mnras/stab3228](https://doi.org/10.1093/mnras/stab3228)
- Lu, S., Xu, D., Wang, Y., et al. 2021, MNRAS, 503, 726, doi: [10.1093/mnras/stab497](https://doi.org/10.1093/mnras/stab497)
- Lu, S., Xu, D., Wang, S., et al. 2022b, MNRAS, 509, 2707, doi: [10.1093/mnras/stab3169](https://doi.org/10.1093/mnras/stab3169)
- Lu, Y. S., Mandelker, N., Oh, S. P., et al. 2024, MNRAS, 527, 11256, doi: [10.1093/mnras/stad3779](https://doi.org/10.1093/mnras/stad3779)
- Maller, A. H., & Dekel, A. 2002, MNRAS, 335, 487, doi: [10.1046/j.1365-8711.2002.05646.x](https://doi.org/10.1046/j.1365-8711.2002.05646.x)
- Maller, A. H., Dekel, A., & Somerville, R. 2002, MNRAS, 329, 423, doi: [10.1046/j.1365-8711.2002.04983.x](https://doi.org/10.1046/j.1365-8711.2002.04983.x)
- Marinacci, F., Vogelsberger, M., Pakmor, R., et al. 2018, MNRAS, 480, 5113, doi: [10.1093/mnras/sty2206](https://doi.org/10.1093/mnras/sty2206)
- Martizzi, D., Vogelsberger, M., Artale, M. C., et al. 2019, MNRAS, 486, 3766, doi: [10.1093/mnras/stz1106](https://doi.org/10.1093/mnras/stz1106)
- Mo, H. J., Mao, S., & White, S. D. M. 1998, MNRAS, 295, 319, doi: [10.1046/j.1365-8711.1998.01227.x](https://doi.org/10.1046/j.1365-8711.1998.01227.x)
- Naiman, J. P., Pillepich, A., Springel, V., et al. 2018, MNRAS, 477, 1206, doi: [10.1093/mnras/sty618](https://doi.org/10.1093/mnras/sty618)
- Nelson, D., Pillepich, A., Springel, V., et al. 2018, MNRAS, 475, 624, doi: [10.1093/mnras/stx3040](https://doi.org/10.1093/mnras/stx3040)
- . 2019a, MNRAS, 490, 3234, doi: [10.1093/mnras/stz2306](https://doi.org/10.1093/mnras/stz2306)
- Nelson, D., Springel, V., Pillepich, A., et al. 2019b, Computational Astrophysics and Cosmology, 6, 2, doi: [10.1186/s40668-019-0028-x](https://doi.org/10.1186/s40668-019-0028-x)
- Neyrinck, M., Aragon-Calvo, M. A., Falck, B., Szalay, A. S., & Wang, J. 2020, The Open Journal of Astrophysics, 3, 3, doi: [10.21105/astro.1904.03201](https://doi.org/10.21105/astro.1904.03201)
- Peebles, P. J. E. 1969, ApJ, 155, 393, doi: [10.1086/149876](https://doi.org/10.1086/149876)

- Pérez-Montaño, L. E., Cervantes Sodi, B., Rodríguez-Gomez, V., Zhu, Q., & Ogiya, G. 2024, MNRAS, 533, 93, doi: [10.1093/mnras/stae1793](https://doi.org/10.1093/mnras/stae1793)
- Pérez-Montaño, L. E., Rodríguez-Gomez, V., Cervantes Sodi, B., et al. 2022, MNRAS, 514, 5840, doi: [10.1093/mnras/stac1716](https://doi.org/10.1093/mnras/stac1716)
- Pichon, C., & Bernardeau, F. 1999, A&A, 343, 663, doi: [10.48550/arXiv.astro-ph/9902142](https://doi.org/10.48550/arXiv.astro-ph/9902142)
- Pichon, C., Pogosyan, D., Kimm, T., et al. 2011, MNRAS, 418, 2493, doi: [10.1111/j.1365-2966.2011.19640.x](https://doi.org/10.1111/j.1365-2966.2011.19640.x)
- Pillepich, A., Nelson, D., Hernquist, L., et al. 2018, MNRAS, 475, 648, doi: [10.1093/mnras/stx3112](https://doi.org/10.1093/mnras/stx3112)
- Pillepich, A., Nelson, D., Springel, V., et al. 2019, MNRAS, 490, 3196, doi: [10.1093/mnras/stz2338](https://doi.org/10.1093/mnras/stz2338)
- Planck Collaboration, Ade, P. A. R., Aghanim, N., et al. 2016, A&A, 594, A13, doi: [10.1051/0004-6361/201525830](https://doi.org/10.1051/0004-6361/201525830)
- Rodríguez-Gomez, V., Sales, L. V., Genel, S., et al. 2017, MNRAS, 467, 3083, doi: [10.1093/mnras/stx305](https://doi.org/10.1093/mnras/stx305)
- Romanowsky, A. J., & Fall, S. M. 2012, ApJS, 203, 17, doi: [10.1088/0067-0049/203/2/17](https://doi.org/10.1088/0067-0049/203/2/17)
- Romeo, A. B., Agertz, O., & Renaud, F. 2023, MNRAS, 518, 1002, doi: [10.1093/mnras/stac3074](https://doi.org/10.1093/mnras/stac3074)
- Sawala, T., Frenk, C. S., Fattahi, A., et al. 2016, MNRAS, 457, 1931, doi: [10.1093/mnras/stw145](https://doi.org/10.1093/mnras/stw145)
- Schäfer, B. M. 2009, International Journal of Modern Physics D, 18, 173, doi: [10.1142/S0218271809014388](https://doi.org/10.1142/S0218271809014388)
- Sharma, S., Steinmetz, M., & Bland-Hawthorn, J. 2012, ApJ, 750, 107, doi: [10.1088/0004-637X/750/2/107](https://doi.org/10.1088/0004-637X/750/2/107)
- Sousbie, T. 2011, MNRAS, 414, 350, doi: [10.1111/j.1365-2966.2011.18394.x](https://doi.org/10.1111/j.1365-2966.2011.18394.x)
- Sousbie, T., Pichon, C., & Kawahara, H. 2011, MNRAS, 414, 384, doi: [10.1111/j.1365-2966.2011.18395.x](https://doi.org/10.1111/j.1365-2966.2011.18395.x)
- Springel, V. 2010, MNRAS, 401, 791, doi: [10.1111/j.1365-2966.2009.15715.x](https://doi.org/10.1111/j.1365-2966.2009.15715.x)
- Springel, V., White, S. D. M., Tormen, G., & Kauffmann, G. 2001, MNRAS, 328, 726, doi: [10.1046/j.1365-8711.2001.04912.x](https://doi.org/10.1046/j.1365-8711.2001.04912.x)
- Springel, V., Pakmor, R., Pillepich, A., et al. 2018, MNRAS, 475, 676, doi: [10.1093/mnras/stx3304](https://doi.org/10.1093/mnras/stx3304)
- Stewart, K. R., Brooks, A. M., Bullock, J. S., et al. 2013, ApJ, 769, 74, doi: [10.1088/0004-637X/769/1/74](https://doi.org/10.1088/0004-637X/769/1/74)
- Stewart, K. R., Kaufmann, T., Bullock, J. S., et al. 2011, ApJ, 738, 39, doi: [10.1088/0004-637X/738/1/39](https://doi.org/10.1088/0004-637X/738/1/39)
- Tacchella, S., Dekel, A., Carollo, C. M., et al. 2016, MNRAS, 457, 2790, doi: [10.1093/mnras/stw131](https://doi.org/10.1093/mnras/stw131)
- Teklu, A. F., Remus, R.-S., Dolag, K., et al. 2015, ApJ, 812, 29, doi: [10.1088/0004-637X/812/1/29](https://doi.org/10.1088/0004-637X/812/1/29)
- Tillson, H., Devriendt, J., Slyz, A., Miller, L., & Pichon, C. 2015, MNRAS, 449, 4363, doi: [10.1093/mnras/stv557](https://doi.org/10.1093/mnras/stv557)
- Valenzuela, L. M., & Remus, R.-S. 2024, A&A, 686, A182, doi: [10.1051/0004-6361/202244758](https://doi.org/10.1051/0004-6361/202244758)
- Vitvitska, M., Klypin, A. A., Kravtsov, A. V., et al. 2002, ApJ, 581, 799, doi: [10.1086/344361](https://doi.org/10.1086/344361)
- Wang, L., De Lucia, G., Fontanot, F., & Hirschmann, M. 2019, MNRAS, 482, 4454, doi: [10.1093/mnras/sty2998](https://doi.org/10.1093/mnras/sty2998)
- Wang, S., Xu, D., Lu, S., et al. 2022, MNRAS, 509, 3148, doi: [10.1093/mnras/stab3167](https://doi.org/10.1093/mnras/stab3167)
- Wang, S., Xu, D., Lu, S., & Li, C. 2024, MNRAS, 527, 7028, doi: [10.1093/mnras/stad3634](https://doi.org/10.1093/mnras/stad3634)
- Wang, X., Szalay, A., Aragón-Calvo, M. A., Neyrinck, M. C., & Eyink, G. L. 2014, ApJ, 793, 58, doi: [10.1088/0004-637X/793/1/58](https://doi.org/10.1088/0004-637X/793/1/58)
- Welker, C., Devriendt, J., Dubois, Y., Pichon, C., & Peirani, S. 2014, MNRAS, 445, L46, doi: [10.1093/mnras/lu106](https://doi.org/10.1093/mnras/lu106)
- White, S. D. M. 1984, ApJ, 286, 38, doi: [10.1086/162573](https://doi.org/10.1086/162573)
- White, S. D. M., & Rees, M. J. 1978, MNRAS, 183, 341, doi: [10.1093/mnras/183.3.341](https://doi.org/10.1093/mnras/183.3.341)
- Winkel, N., Pasquali, A., Kraljic, K., et al. 2021, MNRAS, 505, 4920, doi: [10.1093/mnras/stab1562](https://doi.org/10.1093/mnras/stab1562)
- Yang, H., Liao, S., Fattahi, A., et al. 2024, MNRAS, 535, 1394, doi: [10.1093/mnras/stae2411](https://doi.org/10.1093/mnras/stae2411)
- Zavala, J., Frenk, C. S., Bower, R., et al. 2016, MNRAS, 460, 4466, doi: [10.1093/mnras/stw1286](https://doi.org/10.1093/mnras/stw1286)
- Zeng, G., Wang, L., & Gao, L. 2021, MNRAS, 507, 3301, doi: [10.1093/mnras/stab2294](https://doi.org/10.1093/mnras/stab2294)
- Zhang, S., Cai, Z., Xu, D., et al. 2023, Science, 380, 494, doi: [10.1126/science.abj9192](https://doi.org/10.1126/science.abj9192)
- Zhu, Q., Pérez-Montaño, L. E., Rodríguez-Gomez, V., et al. 2023, MNRAS, 523, 3991, doi: [10.1093/mnras/stad1655](https://doi.org/10.1093/mnras/stad1655)
- Zjupa, J., & Springel, V. 2017, MNRAS, 466, 1625, doi: [10.1093/mnras/stw2945](https://doi.org/10.1093/mnras/stw2945)